Simulation of the control of vortex breakdown in a closed cylinder using a small rotating disk

Boon Thong Tan,[1,a)] Keith Y. S. Liow,[1] Lewis Mununga,[2] Mark C. Thompson,[2,3] and Kerry Hourigan[2,3]
[1]*School of Engineering, Monash University Malaysia, P.O. Box 8975, 46780 Kelana Jaya, Selangor 46150, Malaysia*
[2]*Department of Mechanical and Aerospace Engineering, Fluids Laboratory for Aeronautical and Industrial Research (FLAIR), Monash University, P.O. Box 31, Clayton Campus, Victoria 3800, Australia*
[3]*Monash University Biomedical Engineering Technology Alliance (MuBeta), Monash University, P.O. Box 31, Clayton Campus, Victoria 3800, Australia*

(Received 8 September 2008; accepted 8 December 2008; published online 5 February 2009)

The enhancement or suppression of vortex breakdown in a closed cylinder caused by a small rotating disk embedded in the nonrotating endwall is simulated in this study. This paper shows that corotation or counter-rotation of the control disk with respect to the driving lid is able to promote or suppress the "bubble-type" vortex breakdown. This is achieved using only a small fraction of the power required to drive the main lid. The simulations show that the vortex breakdown induced or suppressed by flow control displays similar characteristics near the breakdown region as produced by varying the flow Reynolds number. These include near-axis swirl, centerline axial velocity, and centerline pressure. The influence of the size of the control disk is also quantified. © *2009 American Institute of Physics*. [DOI: 10.1063/1.3073747]

I. INTRODUCTION

Since its discovery, vortex breakdown has been studied extensively and numerous reviews have discussed various aspects.[1–10] Several theoretical models have been developed to predict this phenomenon. These include the collapse of the near-axis boundary layer,[6] hydraulic jump analogy,[11,12] internal separation,[7,13] flow instability,[14,15] and a fold catastrophe.[10,16] Vortex breakdown occurs in strongly swirling flows such as those found in unconfined jets and pipes. Although perhaps these have more obvious practical applications, vortex breakdown in a confined cylinder has also been extensively studied because the flow conditions can be precisely controlled. However, perhaps surprisingly, the flow is extremely sensitive to perturbations to the geometry of the rig and imperfect visualization techniques, which can cause substantial differences between numerical predictions and experimental results.[17–19] Apart from its use as a tool to provide a theoretical understanding, the confined cylinder rig may provide a useful prototype bioreactor for the growth of various cell types.[20–23]

The confined flow is governed by only two parameters, i.e., the flow Reynolds number Re_D and the aspect ratio H/R, where H and R are the cylinder height and radius, respectively. Vogel[24] first observed vortex breakdown in this flow configuration. Flow states with up to three vortex breakdown bubbles have been mapped out.[25] Studies have shown that vortex breakdown in a confined cylinder is axisymmetric and steady at low Reynolds numbers.[18,19] The development of a steady axisymmetric vortex breakdown bubble formed by increasing the Reynolds number of the axisymmetric flow has been shown to be a continuous evolution.[4]

Numerous techniques for controlling vortex breakdown have been explored. Mitchell and Délery[26] examined the control of vortex breakdown for trailing vortices from delta wings. In a closed cylinder, techniques employed include temperature gradients,[27] corotating,[28,29] and counter-rotating end walls,[30] and independently rotating a small central rod.[31] Lopez *et al.*[32] studied how harmonic oscillations can be used to control the vortex breakdown bubble at higher Reynolds numbers where the flow is unsteady and axisymmetric.

A mechanical and nonintrusive method is used in this study to control axisymmetric vortex breakdown in a confined cylinder. A small rotating disk on the end opposite to the driving lid is used to control vortex breakdown. Control is applied by varying only the boundary conditions while avoiding any protuberances in the flow. This study complements the experimental investigation undertaken by Mununga *et al.*[33]

There are various descriptions and definitions of vortex breakdown in the literature. A simple definition proposed by Leibovich[7] describes vortex breakdown as a substantial change in the structure of the vortex core as a direct result of a variation in the characteristic ratio of the tangential to axial velocity components. Accordingly, in the present study vortex breakdown control can be interpreted as being achieved by altering the swirl and/or axial velocity near the central core. Corotation or counter-rotation of a small disk increases or decreases the swirl velocity near the axis, respectively. The axial velocity near the breakdown position will be shown later to decrease, in both cases.

A layout of the flow configuration is shown in Fig. 1. The container has an overall diameter of D (radius R) and a height of H. The radial distance r is measured from the rotational axis and the axial position z is measured from the

[a)]Electronic mail: tan.boon.thong@eng.monash.edu.my.

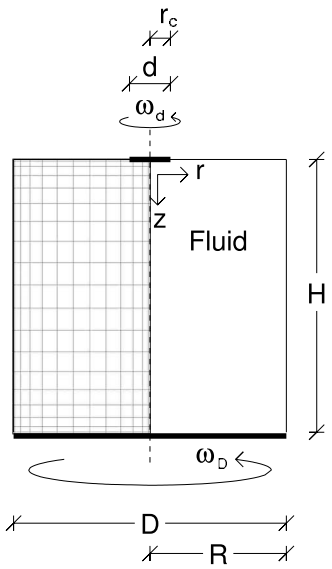

FIG. 1. Schematic showing the cylinder, driving lid, and control disk. The spectral-element macromesh used for the computations is shown in the left-hand section of this figure.

control disk. The aspect ratio used in this study is $H/R=2$, in line with many previous studies (e.g., Refs. 4, 25, and 33). The main disk driving the flow constitutes the entire lid (i.e., radius R) and rotates at an angular speed of ω_D. The smaller control disk is embedded into the opposite lid and rotates about the same axis. The diameter d (radius r_c) of the control disk is fixed at $d=0.15D$ ($r_c=0.15R$) in all cases except in a later section that studies the effects of varying the size of the control disk. This value is chosen for consistency with the experimental study.[33] The Reynolds number of the flow, Re_D, is based on the radius and the rotational speed of the main driving disk,

$$\mathrm{Re}_D = \frac{\omega_D R^2}{\nu}, \tag{1}$$

with ν the kinematic viscosity of the fluid. The Reynolds number of the flow in this study is chosen to lie in the vicinity where the vortex breakdown bubble is first observed (i.e., close to the onset value for vortex breakdown). To reiterate, the formation of a vortex breakdown bubble is not associated with an instability or a bifurcation.[4] For this geometry and aspect ratio, the onset of vortex breakdown occurs when the Reynolds number is $\mathrm{Re}_D \approx 1440$, and the flows simulated in this study are all within approximately $\mathrm{Re}_D \pm 500$ of this onset value. This range lies below the critical Re_D at which the flow becomes unsteady in time or develops spiral modes.[19]

The Reynolds number associated with the control disk is defined as

$$\mathrm{Re}_d = \frac{\omega_d r_c^2}{\nu}. \tag{2}$$

The speeds of the control disk for both co- and counter-rotations are kept to moderate levels relative to the main lid, with rotation ratios restricted to $|\omega_d/\omega_D| < 4.5$ for cases where $d/D=0.15$. Generally, the Reynolds numbers of the control disk never exceed $|\mathrm{Re}_d| < 150$. Positive and negative values for Re_d and ω_d/ω_D represent corotation and counter-rotation, respectively.

This paper extends the preliminary experimental study in the brief communication of Ref. 33 in a number of ways. In particular, it presents detailed numerical simulations extending the previous experimental study by providing circulation, vorticity, and pressure maps, which in turn provide a physical understanding of the effect of the control disk. Indeed, the control disk increases or decreases the swirl velocity upstream of breakdown, depending on the rotation direction, but always decreases the axial velocity. This allows enhancement or inhibition of breakdown to be interpreted in terms of a change to the upstream *swirl number*. In addition, the input power to drive each disk is properly quantified, and the effect of the size of the control disk is determined.

The layout of the remainder of this paper is as follows. The numerical techniques, relevant equations, and parameters used to model the flow are presented in Sec. II. This is followed by validation of the model against experimental data. The flows generated independently by the top and bottom rotating disks are then documented. The effect of co- and counter-rotations of the control disk on the flow is studied by investigating the axial velocity along the centerline, the circulation in the vicinity of the vortex breakdown bubble, and the pressure along the central axis. The shape of the vortex breakdown bubble for a selection of cases is shown using streamline plots. The powers required to drive both the main disk and the control disk are calculated to highlight the high efficiency of this control mechanism. Several sizes of control disk are also simulated to study the relationship between the size of the control disk and the power required to instigate and suppress vortex breakdown. Finally a brief discussion and conclusion follows.

II. NUMERICAL METHOD

The flow is assumed to be axisymmetric at the low Reynolds numbers considered in this study. All results presented here reached a steady asymptotic state. This reduces the problem to only two spatial dimensions. The flow field is modeled by solving the incompressible time-dependent Navier–Stokes equation in cylindrical polar coordinates. A spectral-element method is used for the axisymmetric geometry and the solution is advanced in time using a time splitting technique that is second-order accurate. This technique and the implementation have been validated and have been used extensively for various related problems, e.g., Refs. 19, 34, and 35.

The computational mesh used in this study is also shown in Fig. 1. This mesh consists of 13×19 *macroelements*. Each macroelement in this plot contains a further 10×10 computational nodes (not shown). The mesh is stretched using a Chebyshev (cosine) function to concentrate points toward each boundary. Stretching toward the solid boundary is required for better resolution of the thin boundary layers, especially the Ekman layer at the spinning-lid wall and the Stewartson layer at the sidewalls. In addition, better resolution of the vortex breakdown bubble is achieved by concentrating points toward the axis. A linear velocity profile is

imposed on the bottom boundary to enforce a constant angular velocity of ω_D. A no-slip boundary condition is imposed on the stationary walls. A linear velocity profile matching the desired angular velocity of the control disk is imposed at the surface of the control disk.

The mesh stretching used in this study results in a high mesh density near the corners of the domain. The singularity here resulting from the discontinuity in imposed velocity and/or geometry leads to a loss in spectral convergence. The high local mesh density in these regions isolates the unnatural oscillations from propagating to the rest of the flow domain.

For computational efficiency, simulations are generally initialized with a solution from a lower Reynolds number case when one is available. Simulations with a rotating control disk are started with a solution at the same Re_D but with the control disk stationary. The simulations are then integrated forward in time using a time step of $\omega_D \Delta t = 0.015$ for $\mathrm{Re}_D \leq 1500$ and $\omega_D \Delta t = 0.01$ for cases with higher Reynolds number. As indicated above, all cases considered in this study asymptote to a steady state which typically requires several hundred dynamic time units ($1/\omega_D = 1$ time unit). The flow is considered to be steady when the largest variation in any component of velocity at any node is less than $\Delta u / \Delta t \omega_D^2 R < 10^{-6}$.

Simulations were performed with a higher resolution and with a smaller time step to verify that the solutions were accurate. Tests were performed for the cases between $\mathrm{Re}_D = 1500$ and $\mathrm{Re}_D = 2500$. The same computational mesh was used but with higher-order elements containing 13×13 computational nodes. The time step was reduced to $\omega_D \Delta t = 0.01$ for $\mathrm{Re}_D \leq 1800$ and $\omega_D \Delta t = 0.005$ for cases with higher Re_D. The size and location of the vortex breakdown bubble were used for verification. The location of the upstream and downstream stagnation points on the vortex breakdown bubble varied by less than 0.25% of H. The width of the bubble at its widest varied by less than 0.3%. Given these results, the (base) resolution and time step are adequate to produce accurate predictions.

Of interest to the aspect of control is the power input required to significantly modify the breakdown bubble relative to the input power to generate breakdown. The shaft power $\dot{W}_{\mathrm{shaft}}$ required to rotate either the main lid or the control lid is given by

$$\dot{W}_{\mathrm{shaft}} = \left| \int \mu \frac{\partial u_\theta}{\partial z} u_\theta dA \right|. \tag{3}$$

The velocity in the azimuthal direction is represented by u_θ and the dynamic viscosity is represented by μ. For an axisymmetric problem, the area integral can be reduced to a line integral,

$$\dot{W}_{\mathrm{shaft}} = \left| \int_0^R 2\pi\mu \frac{\partial u_\theta}{\partial z} u_\theta r dr \right|. \tag{4}$$

Note that taking the limits of integration to R rather than r_c does not affect the result because the stationary portion does not contribute to any shaft work. Integration is done using the same numerical quadrature as used in the spectral-element scheme. The nondimensional power coefficient is scaled with the properties of the main driving lid and given by

$$C_P = \frac{\dot{W}_{\mathrm{shaft}}}{\rho \omega_D^3 R^5}. \tag{5}$$

Here, the density of the fluid is represented by ρ.

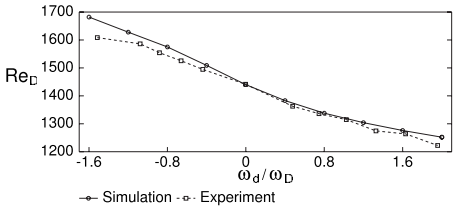

FIG. 2. The Reynolds number (Re_D) associated with the onset of vortex breakdown, as a function of the rotation ratio of the control disk to the rotating lid (ω_d/ω_D). Note that negative values of ω_d/ω_D indicate counter-rotation.

III. RESULTS AND DISCUSSION

A. Experimental validation

In order to validate the numerical predictions, a preliminary series of simulations was performed and the results compared with those from an experimental study.[33] In this exercise, the rotational speed of the control lid relative to the driving lid was varied between $-1.6 \leq \omega_d/\omega_D \leq 2.0$, and the Re_D at the onset of vortex breakdown was determined. In the numerical study, simulations were performed at increments as fine as 1 unit of Re_D by varying the kinematic viscosity and the onset was deemed to have occurred when flow reversal on the central axis was detected. On the experimental side, Re_D was varied by minute increments in motor speed and the vortex breakdown was detected visually.

The graph in Fig. 2 shows a comparison of the numerical and experimental predictions. The overall agreement is good and the deviation never exceeds 4% and is mostly better than 1%. The likely source of the difference is in different ways the breakdown bubble is detected between the experiments and numerics. Clearly, the detection of the onset of reverse flow on the axis in the numerical simulations is more definitive than visual inspection. In any case, the two sets of results are in excellent agreement.

B. Flow induced by the primary and control disks

The separate flows induced by rotation of the primary and control disks are documented in this section. This is done by keeping one disk stationary and rotating the other disk.

Viscous forces transfer momentum from the rotational lid at the bottom to the entire container of fluid. The swirl or azimuthal flow induces flow radially outward. The stronger swirl near the lower lid drives the secondary flow in the clockwise direction as shown by the streamline plot on the meridional plane in Fig. 3(a). Arrows have been added to highlight the downward motion of the secondary flow near the cylinder axis.

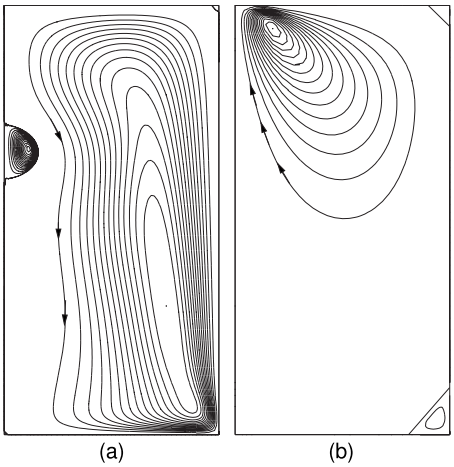

FIG. 3. Plots showing (a) the streamlines at $Re_D=1600$ and the control disk (top) stationary and (b) streamlines for $Re_d=60$ with the driving lid (bottom) stationary.

The same mechanism also applies to the secondary flow induced by the control disk as shown in Fig. 3(b). The disk is smaller and the flow is weaker in this case. The control disk on the opposite side of the driving lid induced flow is in the counterclockwise direction. Again, arrows have been added to show that the induced flow near the axis is in the upward direction. The direction of the secondary flow on the meridional plane is independent of the direction of rotation.

The resultant flow from both the rotating lid and the control disk is not a simple superposition due to the nonlinear nature of the system. However, the control flow is expected to reduce the axial velocity due to their opposing directions. Section III C will show this to be the case for both corotation and counter-rotation of the control disk.

C. Effect of the control disk

Vortex breakdown control is investigated through three sets of simulations. For the base case, the Reynolds number Re_D is increased past the onset of vortex breakdown with no external flow control applied. Next, a Reynolds number well below the onset of vortex breakdown is chosen (i.e., $Re_D=1200$, approximately 20% below the onset of vortex breakdown) with corotation of the control disk used to promote vortex breakdown. Finally, a Reynolds number above onset is selected (i.e., $Re_D=1835$, about 20% above the onset of vortex breakdown) and counter-rotation of the control disk is used to suppress vortex breakdown. Note that the actual Reynolds numbers were chosen to match with experiments.

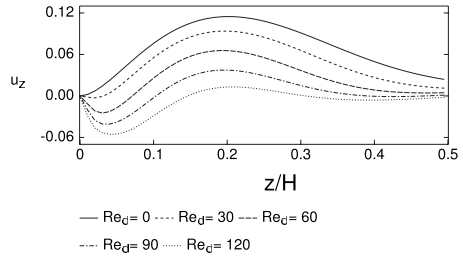

FIG. 5. The axial velocity (u_z) along the centerline as a function of distance from the control disk (z/H) for various Re_d (corotation). $Re_D=1200$.

Initially, the axial velocity along the axis and the swirl close to the axis is studied because the swirl number is dependent on these, and that has been shown to be a useful predictor of downstream breakdown. The swirl number is defined as the ratio of swirl velocity to the axial velocity. While the axial velocity should not be too sensitive to radial position close to the axis, for axisymmetric flows the swirl velocity will vary linearly near the axis, hence there is some arbitrariness in specifying what swirl velocity should be used to construct the swirl number. In the analysis of breakdown of a swirling jet issuing into an otherwise quiescent fluid, Chomaz *et al.*[36] found that the swirl velocity reached a maximum at the edge of the jet, so providing a natural swirl velocity scale for constructing a swirl number. They found that breakdown would occur downstream if their swirl number exceeded approximately 1.4. For the spinning-lid rig, there is no well defined swirling jet core upstream of breakdown. The finer details of how this measurement is taken are dependent on the actual flow configuration. In this case, the axial velocity along the axis and in the vicinity of the vortex breakdown bubble is used as a gauge. Circulation, which is defined as $\Gamma=u_\theta r$, is used as an indication of the strength of the swirl.

The pressure along the centerline is examined next. The topology of the vortex breakdown structure and the power requirements to generate the flow is also considered.

1. Axial velocity

Figure 4–6 show plots of axial velocity (u_z) along the axis for the top half of the vessel. Figure 4 shows the effect of varying the Reynolds number Re_D when no flow control is applied. As Re_D is increased, there is a drop in axial velocity,

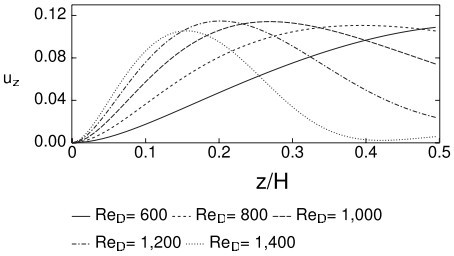

FIG. 4. The axial velocity (u_z) along the centerline as a function of distance from the control disk (z/H) with the control disk stationary.

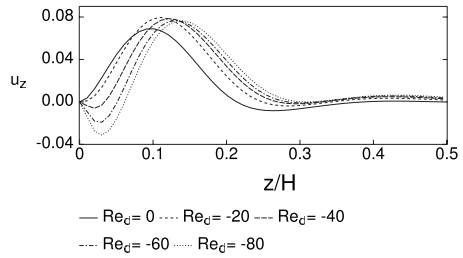

FIG. 6. The axial velocity (u_z) along the centerline as a function of distance from the control lid (z/H) for various Re_d (counter-rotation) and $Re_D=1835$.

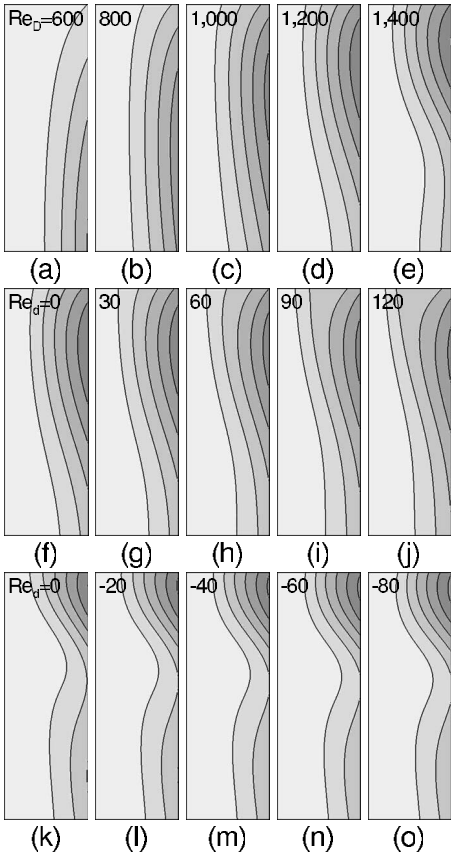

FIG. 7. Plots of circulation ($\Gamma = u_\theta r$) for various cases. Control disk is stationary and (a) $\mathrm{Re}_D = 600$, (b) 800, (c) 1000, (d) 1200, and (e) 1400. Flow at $\mathrm{Re}_D = 1200$ and the corotating control disk speed varied, (f) $\mathrm{Re}_d = 0$, (g) 30, (h) 60, (i) 90, and (j) 120. Flow at $\mathrm{Re}_D = 1835$ and the counter-rotating control disk speed varied, (k) $\mathrm{Re}_d = 0$, (l) −20, (m) −40, (n) −60, and (o) −80. The contours are at intervals of $\Gamma/(\omega_D R^2) = 0.005$ starting from 0 at the axis.

especially near $z/H \approx 0.37$. A vortex breakdown bubble forms in this region when the velocity drops below zero, signifying flow reversal. The corotation case is represented by $\mathrm{Re}_D = 1200$ and shown in Fig. 5. The effect of the control disk is clearly to reduce the axial velocity in its vicinity ($0 < z/H < 0.1$). The axial velocity further away is also reduced and flow reversal associated with vortex breakdown first occurs between $80 < \mathrm{Re}_d < 90$ at $z/H \approx 0.44$. The flow at $\mathrm{Re}_D = 1835$ is chosen to represent the counter-rotation case. The control disk also reduces the axial velocity in the near region (i.e., $0 < z/H < 0.1$), similar to the corotation case. Counter-rotation increases axial velocity further away from the disk and vortex breakdown suppression starts between $-80 < \mathrm{Re}_d < -70$.

2. Circulation

Circulation ($\Gamma = u_\theta r$) contour plots for a selection of cases are presented in Fig. 7. The viewing window spans the ranges between $0 < r/R < 0.3$ and $0.1 < z/H < 0.55$, thus focusing on the vortex breakdown region. Strong swirl near the axis would result in higher levels of circulation. Therefore, higher contouring levels nearer to the axis represent stronger swirl. Figures 7(a)–7(e) represent increasing Reynolds number Re_D with the control disk stationary. These plots show

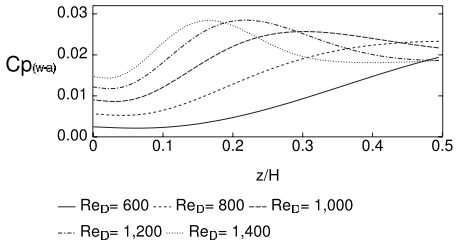

FIG. 8. The pressure coefficient ($C_{p(w-a)}$) along the centerline as a function of distance from the control lid (z/H) with the control lid stationary.

that circulation near the axis grows as Reynolds number is increased. The plots in Figs. 7(f)–7(j) correspond to $\mathrm{Re}_D = 1200$ with vortex breakdown induced by corotation of the control disk. The plots also show an increase in circulation near the axis, although less significant than the earlier case. Finally, suppression of vortex breakdown at $\mathrm{Re}_D = 1835$ is shown by plots in Figs. 7(k)–7(o), ordered in terms of increasing control disk speeds. In this case, the circulation near the axis decreases as the counter-rotation speed increases.

3. Pressure along the centerline

A region of low pressure relative to the two lids along the rotating axis is a necessary condition for vortex breakdown.[31] Plots of the pressure coefficient along the axis will be shown here to highlight the effects of the control flow. The pressure along the axis is taken relative to the pressure on the wall. The pressure coefficient is defined as

$$c_P = \frac{P_w - P_a}{\frac{1}{2}\rho\omega_D^2 R^2}. \tag{6}$$

Here, P_w is the pressure on the wall, P_a is the pressure at the axis, and ρ is the fluid density. To obtain a positive value for the pressure coefficient, the pressure at the wall is subtracted from the pressure at the axis.

Figure 8 shows the cases when the control disk is stationary. The pressure along the axis in the region of $0 < z/H < 0.2$ drops as the Reynolds number (Re_D) is increased. A distinct peak is observed at $z/H \approx 0.16$ for $\mathrm{Re}_D = 1400$. This corresponds to the stronger swirl near the axis as seen in Fig. 7 in Sec. III B. The suction pressure reduces further downstream for cases with higher Re_D. This corresponds to lower circulation further downstream and is highlighted in Fig. 7(d) for the case with $\mathrm{Re}_D = 1400$.

The effect of corotation can be seen in Fig. 9. As the speed of the control disk increases, the pressure drops in the

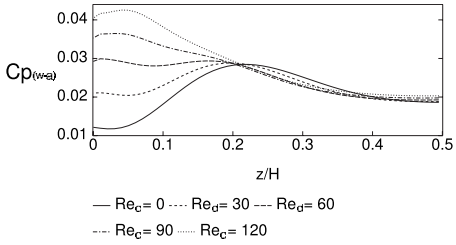

FIG. 9. The pressure coefficient ($C_{p(w-a)}$) along the centerline as a function of distance from the control lid (z/H) when $\mathrm{Re}_D = 1200$.

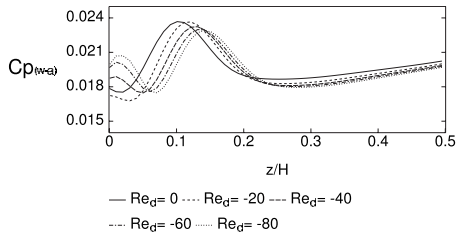

FIG. 10. The pressure coefficient ($C_{p(w-a)}$) along the centerline as a function of distance from the control lid (z/H) when $\mathrm{Re}_D=1835$.

vicinity of $0<z/H<0.2$. This low pressure is associated with the increase in swirl contributed by the control disk. The control flow has little effect on pressure past $z/H>0.2$. This demonstrates that the effect of the control disk is localized.

The counter-rotation case is presented in Fig. 10. The pressure drop increases in the localized region of $z/H<0.07$ due to the rotation of the control disk. The plots clearly reflect a drop in suction past this region. This is related to the net effect of the control disk reducing the level of swirl.

D. Structure of vortex breakdown bubble

The Reynolds number Re_D is increased past the onset of vortex breakdown in this section to show the structure of the vortex breakdown bubble. Streamline plots from selected cases are presented in Fig. 11. Consistent with previous plots, the viewing window spans only between $0<r/R<0.3$ and $0.1<z/H<0.55$ and focuses on the vortex breakdown region. Note that finer contouring levels are used for the counterclockwise flow.

The case with no flow control is shown in Figs. 11(a)–11(e). As the Reynolds number is increased, the vortex breakdown bubble increases in size and moves upstream. If we use the zero streamline as the boundary of the vortex breakdown bubble, at $\mathrm{Re}=1800$, the bubble width is $r/R=0.22$.

The flow Reynolds number is fixed at $\mathrm{Re}_D=1441$ in Figs. 11(f)–11(j), which is at the onset of vortex breakdown. The vortex breakdown is promoted by corotation of the control disk. As the speed of the control disk is increased, the width of the vortex breakdown bubble increases. At $\mathrm{Re}_d=80$, the width of the bubble is at $r/R=0.173$. The vortex breakdown bubble formed here is more elongated because of the reduced axis velocity introduced by the control flow.

Figures 11(k)–11(o) show the vortex breakdown being suppressed by counter-rotation. These plots are arranged in decreasing speed of the control disk so that an easy comparison can be made with the earlier cases. With regards to the shape of the vortex breakdown bubble, increasing the speed of the control disk is similar to decreasing the Reynolds number Re_D of the flow in the case where the disk is stationary [see Figs. 11(a)–11(e)].

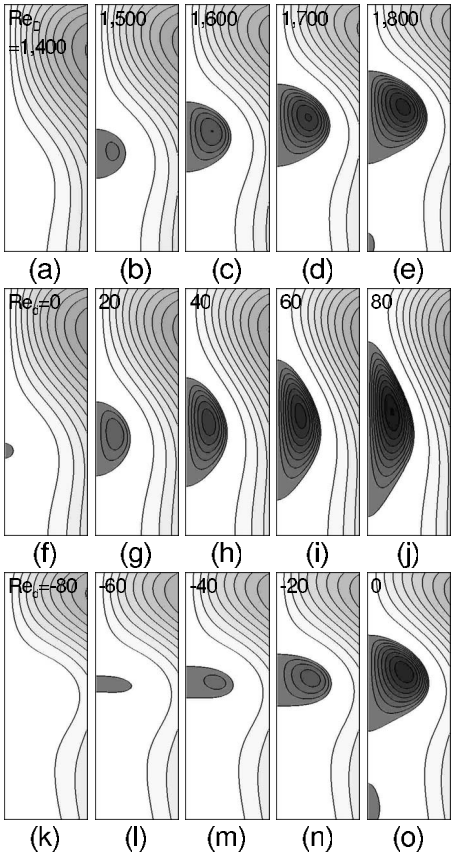

FIG. 11. Plots of stream function for various cases. Control disk stationary and (a) $\mathrm{Re}_D=1400$, (b) 1500, (c) 1600, (d) 1700, and (e) 1800. Flow at $\mathrm{Re}_D=1441$ and the corotating control disk varied, (f) $\mathrm{Re}_d=0$, (g) 20, (h) 40, (i) 60, and (j) 80. Flow at $\mathrm{Re}_D=1835$ and the counter-rotating control disk varied, (k) $\mathrm{Re}_d=-80$, (l) -60, (m) -40, (n) -20, and (o) 0. The lighter/darker shades represent flow in the anticlockwise/clockwise direction and contoured at intervals of $\Phi/(\omega_D R^2)=1\times10^{-3}/1.5\times10^{-5}$.

E. Power requirements

The power predicted to drive the lid and the control disk is presented in this section. The method used to calculate the power coefficient is presented earlier in Sec. II.

The power coefficient required to drive the main lid is presented in Fig. 12. The curve shows that the relationship between the power coefficient and Reynolds number is approximately

$$C_P \propto \mathrm{Re}_D^{-0.7}. \tag{7}$$

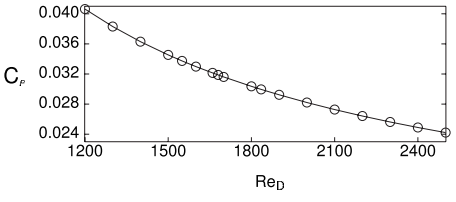

FIG. 12. Power coefficient (C_P) require to drive the lid as a function of Re_D when the control disk is stationary.

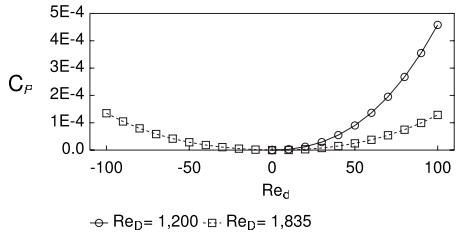

FIG. 13. Power coefficient (C_P) required to drive the control lid as a function of Re_d when the flow is at Re_D=1200 and 1835.

Consider a typical case where the properties of the fluid and geometry of the vessel are fixed. Then Re_D is increased by increasing the rotational speed of the lid. In that case, the shaft power required and rotational speed or Reynolds number now show this approximate relationship,

$$\dot{W}_{\text{shaft}} \propto \Omega_D^{2.3} \propto \text{Re}_D^{2.3}. \tag{8}$$

In all the simulations performed in this study, the speed of the control disk has a negligible effect on the power requirements for the driving lid (i.e., less than 1%). Therefore the power requirements for the driving lid are independent of the rotational speed of the control disk.

The power required to drive the control disk for both Re_D=1200 and 1835 is presented in Fig. 13. The power coefficient is still based on the driving lid. The power coefficient for the control disk at Re_D=1835 is lower than at Re_D=1200 because of the relatively smaller effect of viscosity at higher Re_D. The plot also shows a negligible difference between corotation and counter-rotation for Re_D=1835. Note from the vertical axes in the plot that the control lid requires approximately two orders of magnitude less power than the driving lid.

F. Effects of varying the size of the control disk

Three different control disk sizes, namely d/D=0.1, 0.15, and 0.3, were used to induce vortex breakdown at a Reynolds number below the onset of vortex breakdown of Re_D=1200 with corotation and to suppress vortex breakdown at a Reynolds number above the onset of vortex breakdown of Re_D=1835 with counter-rotation. The speed of the control disk was incremented by 1 unit in Re_d until vortex breakdown was observed at Re_D=1200 or vortex breakdown was suppressed at Re=1835. Flow reversal of axial velocity along the centerline was used as an indication of the presence of vortex breakdown. Tables I and II summarize the results at Re_D=1200 and Re=1835, respectively.

TABLE I. The onset of vortex breakdown induced by the control disk at Re_D=1200.

d/D	0.1	0.15	0.3
Re_d	137	89	50
ω_d/ω_D	11.42	3.30	0.46
C_P (main disk)	4.06×10^{-2}	4.07×10^{-2}	4.06×10^{-2}
C_P (control disk)	1.42×10^{-3}	3.46×10^{-4}	3.92×10^{-5}

TABLE II. The suppression of vortex breakdown by the control disk at Re_D=1835.

d/D	0.1	0.15	0.3
Re_d	144	79	20
ω_d/ω_D	−12	−2.93	−0.19
C_P (main disk)	3.00×10^{-2}	3.00×10^{-2}	3.00×10^{-2}
C_P (control disk)	4.54×10^{-4}	7.42×10^{-5}	4.77×10^{-6}

The results show that as the size of the disk increases, the Re_d and rotational speed required either to promote vortex breakdown at Re_D=1200 or suppress vortex breakdown at Re_D=1835 decreases significantly. This results in the power required to drive the control lid to reduce by approximately two orders in magnitude when the size of the control disk is increased from d/D=0.1 to 0.3. The power required to drive the main disk is approximately constant in each of these cases.

IV. DISCUSSION

The case with no external control is consistent with many previous studies (e.g., Ref. 25). As the Reynolds number is increased, the axial velocity in the core drops and this is most significant near the vortex breakdown region. Plots of circulation also show that the swirl gets stronger and this results in a lower pressure in the core. As the Reynolds number is increased past the onset of vortex breakdown, the vortex breakdown bubble increases in radius and moves a small distance upstream.

Corotation and counter-rotation of the control disk promotes and suppresses vortex breakdown, respectively. Rotation in either direction promotes flow in the direction opposite to the flow generated by the main driving lid, in the meridional plane. This results in lower axial velocity especially near the control disk (i.e., $z/H<0.1$). Outside this region, corotation reduces the axial velocity further and promotes vortex breakdown. Counter-rotation suppresses vortex breakdown and the axial velocity increases.

The circulation plots clearly show that corotation adds swirl to the core region while counter-rotation reduces it. This is reflected in the lower core pressures in the corotation cases and higher core pressures in the counter-rotation cases. Therefore, corotation increases the swirl number by increasing the swirl in the core region and reducing the axial velocity and thus promoting vortex breakdown. Counter-rotation reduces the swirl near the core, which suppress vortex breakdown. Although the rotating control disk reduces axial velocity, this effect is localized to near the disk; axial velocity actually increases further downstream. Therefore, the swirl number decreases and vortex breakdown is suppressed.

All the simulations presented in this study asymptoted to a steady state. The simulations have showed no effects of resonance even when the rotational speeds of both disk are at

integer multiples of each other in the parameter range that was studied.

The development of bioreactors using the breakdown bubble as a virtual reactor for cell or tissue growth can be aided through the provision of a low power control disk to control the size and location of the bubble.[20,21,23]

V. CONCLUSIONS

Control of vortex breakdown was achieved using a control disk and comparisons were made with an experimental study.[33] Corotation and counter-rotation of the control disk promotes and suppress vortex breakdown, respectively. This is achieved by altering the swirl near the vortex breakdown bubble. Streamline plots of the secondary flow show similar vortex breakdown bubbles in cases where the breakdown is promoted using the control disk and when the breakdown occurs solely due to increasing Re_D. The power requirements of the control disk are negligible when compared with the power requirements of the driving lid. A larger control disk has shown to be more power efficient in controlling vortex breakdown. The control disk may be a useful device to control the flow structures in mixing vessels such as bioreactors.

[1] W. Althaus, C. Brucker, and M. Weimer, *Breakdown of Slender Vortices* (Kluwer Academic, Dordrecht, 1995), pp. 373–426.
[2] J. M. Delery, "Aspects of vortex breakdown," Prog. Aerosp. Sci. **30**, 1 (1994).
[3] M. P. Escudier, "Vortex breakdown: Observations and explanations," Prog. Aerosp. Sci. **25**, 189 (1988).
[4] A. Yu. Gelfgat, P. Z. Bar-Yoseph, and A. Solan, "Stability of confined swirling flow with and without vortex breakdown," J. Fluid Mech. **311**, 1 (1996).
[5] A. Yu. Gelfgat, P. Z. Bar-Yoseph, and A. Solan, "Steady states and oscillatory instability of swirling flow in a cylinder with rotating top and bottom," Phys. Fluids **8**, 2614 (1996).
[6] M. G. Hall, "Vortex breakdown," Annu. Rev. Fluid Mech. **4**, 195 (1972).
[7] S. Leibovich, "The structure of vortex breakdown," Annu. Rev. Fluid Mech. **10**, 221 (1978).
[8] J. M. Lopez, "Axisymmetric vortex breakdown Part 1. confined swirling flow," J. Fluid Mech. **221**, 533 (1990).
[9] J. M. Lopez and A. D. Perry, "Axisymmetric vortex breakdown. Part 3 onset of periodic flow and chaotic advection," J. Fluid Mech. **234**, 449 (1992).
[10] V. Shtern and F. Hussain, "Collapse, symmetry breaking, and hysteresis in swirling flows," Annu. Rev. Fluid Mech. **31**, 537 (1999).
[11] T. B. Benjamin, "Theory of vortex breakdown phenomena," J. Fluid Mech. **14**, 593 (1962).
[12] H. B. Squire, *Rotating Fluids* (Cambridge University Press, Cambridge, 1956), pp. 139–161.
[13] S. Leibovich, "Vortex stability and breakdown," AIAA J. **22**, 1192 (1984).
[14] T. Delbende, J. M. Chomas, and P. Huerre, "Absolute/convective instability in the Batchelor vortex: a numerical study of the linear response," J. Fluid Mech. **355**, 229 (1998).
[15] T. Loiseleux, J. M. Chomaz, and P. Huerre, "The effects of swirl on jets and wakes: Linear stability of the rankine vortex with axial flow," Phys. Fluids **10**, 1120 (1998).
[16] V. Shtern, F. Hussain, and M. Herrada, "New features of swirling jets," Phys. Fluids **12**, 2868 (2000).
[17] A. V. Bisgaard, M. Brons, and J. N. Sorensen, "Vortex breakdown generated by off-axis bifurcation in a cylinder with rotating covers," Acta Mech. **187**, 75 (2006).
[18] K. Hourigan, L. J. W. Graham, and M. C. Thompson, "Spiral streaklines in pre-vortex breakdown region of axisymmetric swirling flows," Phys. Fluids **7**, 3126 (1995).
[19] M. C. Thompson and K. Hourigan, "The sensitivity of steady vortex breakdown bubbles in confined cylinder flows to rotating lid misalignment," J. Fluid Mech. **496**, 129 (2003).
[20] J. Dusting, J. Sheridan, and K. Hourigan, "A fluid dynamics approach to bioreactor design for cell and tissue culture," Biotechnol. Bioeng. **94**, 1196 (2006).
[21] K. Y. S. Liow, B. T. Tan, M. C. Thompson, K. Hourigan, and G. A. Thouas, "In-silico characterisation of the flow inside a novel bifurcator for cell and tissue culture," in *Proceedings of the 16th Australasian Fluid Mechanics Conference*, University of Queensland, Gold Coast, Australia, 3–7 December 2007 (School of Engineering, The University of Queensland, Gold Coast, 2007).
[22] G. A. Thouas, J. Sheridan, and K. Hourigan, "A bioreactor model of mouse tumor progression," J. Biomed. Biotechnol. **2007**, 32754 (2007).
[23] P. Yu, T. S. Lee, Y. Zeng, and T. H. Low, "Fluid dynamics of a microbioreactor for tissue engineering," Fluid Dyn. Mater. Process. **1**, 235 (2005).
[24] H. U. Vogel, "Experimentelle Ergebnisse über die laminare Strömung in einem zylindrischen Gehäuse mit darin rotierender Scheibe," Max-Plank-Institute Bericht 6, 1968.
[25] M. P. Escudier, "Observations of the flow produced in a cylindrical container by a rotating endwall," Exp. Fluids **2**, 189 (1984).
[26] A. M. Mitchell and J. Délery, "Research into vortex breakdown control," Prog. Aerosp. Sci. **37**, 385 (2001).
[27] M. A. Herrada and V. Shtern, "Contol of vortex breakdown by temperaturte gradients," Phys. Fluids **15**, 3468 (2003).
[28] S. Bhattacharyya and A. Pal, "Axisymmetric vortex breakdown in a filled cylinder," Int. J. Eng. Sci. **36**, 555 (1998).
[29] D. T. Valentine and C. C. Jahnke, "Flows induced in a cylinder with both end walls rotating," Phys. Fluids **6**, 2702 (1994).
[30] K. G. Roesner, "Recirculating zones in a cylinder with rotating lid," in *Topological Fluid Mechanics: Proceedings of International Union of Theoretical and Applied Mechanics Symposium*, Cambridge, 1990 (Cambridge University Press, Cambridge, 1990).
[31] H. S. Husain, V. Shtern, and F. Hussain, "Control of vortex breakdown by addition of near-axis swirl," Phys. Fluids **15**, 271 (2003).
[32] J. M. Lopez, Y. D. Cui, F. Marques, and T. T. Lim, "Quenching of vortex breakdown oscillations via harmonic modulation," J. Fluid Mech. **599**, 441 (2008).
[33] L. Mununga, K. Hourigan, and M. C. Thompson, "Confined flow vortex breakdown control using a small rotating disk," Phys. Fluids **16**, 4750 (2004).
[34] M. C. Thompson, K. Hourigan, and J. Sheridan, "Three-dimensional instabilities in the wake of a circular cylinder," Exp. Therm. Fluid Sci. **12**, 190 (1996).
[35] M. C. Thompson, T. Leweke, and M. Provansal, "Kinematics and dynamics of sphere wake transition," J. Fluids Struct. **15**, 575 (2001).
[36] P. Billant, J. M. Chomaz, and P. Huerre, "Experimental study of vortex breakdown in swirling jets," J. Fluid Mech. **376**, 183 (1998).